BASIC SCIENCE

Nanomedicine: Nanotechnology, Biology, and Medicine
37 (2021) 102452

Original Article

nanomedjournal.com

Cell-stiffness and morphological architectural patterns in clinical samples of high grade serous ovarian cancers”

Eros Azzalini, PhD[a,d], Nodira Abdurakhmanova, MSc[b], Pietro Parisse, PhD[b,c], Michele Bartoletti, MD[d,e], Vincenzo Canzonieri, MD[a,d], Giorgio Stanta, MD[a], Loredana Casalis, PhD[b], Serena Bonin, PhD[a,*]

[a]*DSM-Department of Medical Sciences, University of Trieste, Trieste, Italy*
[b]*Elettra Sincrotrone Trieste S.C.p.A., Trieste, Italy*
[c]*IOM-CNR, Trieste, Italy*
[d]*IRCCS CRO Aviano-National Cancer Institute, Aviano, Italy*
[e]*Department of Medicine (DAME), University of Udine, Udine, Italy*

Revised 9 July 2021

Abstract

High grade serous ovarian carcinoma (HGSOC) is recognized as the most frequent type of ovarian cancer and the main cause of ovarian cancer related deaths worldwide. Although homologous recombination deficiency testing has been adopted in the clinical workflow, morphological analysis remains the main diagnostic tool. In this study Atomic Force Microscopy (AFM) was tested in standard hematoxylin and eosin (H&E) stained sections to investigate the biomechanical properties of different architectural growing patterns of HGSOC. Our results showed that AFM was able to discriminate HGSOC morphological growing patterns as well as patients' stage. Micropapillary pattern, which has been associated to poor outcome, had lower Young's moduli. In addition stage IV HGSOC was significantly softer than stage III cancers. Based on our results, AFM analysis could represent an additional tool in HGSOC morphological diagnosis as the biomechanical proprieties of HGSOC were quantitatively associated to tumor staging and architectural pattern.

Key words: AFM; FFPE tissues; HGSOC; Cancer morphological architectures; Young's modulus

High grade serous ovarian carcinoma (HGSOC) is the most common type of epithelial ovarian cancer (EOC).[1] This disease has become a public health concern as the 5-year survival rate has not been lengthened over the past decades because there's still a lack of effective treatments.[2] Several efforts have been made to characterize at molecular level the complexity and heterogeneity of this type of cancer and consequently find prognostic and predictive biomarkers useful for patient's management.[3,4] However, so far, apart from the development of immunohistochemical (IHC) algorithms helpful in the differential diagnosis,[5,6] only molecular testing for homologous recombination system deficiency (HRD) has shown its application in clinics, since patients with this feature might benefit from PARPs inhibitors therapy.[7] As a result of the lack of effective molecular targets, the histological analysis of H&E tissue sections under the optical microscope is still the major and most valuable source of information for the pathologists, as histological features have been proven of prognostic significance in several reports.[8–10]

In the last years, certain groups have shown that HGSOC growing architectural patterns can be associated with specific molecular or histological features and, in particular, that HGSOCs with solid, endometrioid-like or transitional-like pattern (gathered together in a group named SET) have a

Acknowledgments: This study was partially supported by the project HERCULES, funded by the European Union's Horizon 2020 research and innovation program under grant agreement No 667403. L.C. and P.P. thank funds by Regione Friuli Venezia Giulia, within the framework of "Regional Law 17/2004: Contributions for clinical, translational, basic, epidemiological and organizational research" with the project "BioMec—Application of Biomechanical Technologies to IntegrateTraditional Methodologies in the Hospital Context".

Disclosure: The authors acknowledge that part of this study was presented to the EACR 2021 Virtual Congress as a poster entitled Nano-Mechanics to study High Grade Serous Ovarian Cancers.

Declaration of competing interests: The authors declare no conflict of interest.

* Corresponding author at: University of Trieste, DSM- Department of Medical Sciences, Trieste, Italy.
E-mail address: sbonin@units.it. (S. Bonin).

https://doi.org/10.1016/j.nano.2021.102452

Please cite this article as: Azzalini E, et a, Cell-stiffness and morphological architectural patterns in clinical samples of high grade serous ovarian cancers. *Nanomedicine: NBM* 2021;37:102452, https://doi.org/10.1016/j.nano.2021.102452

different behavior compared to those having classic features, namely papillary and micropapillary patterns.[11,12] However, the link between these characteristics and patient's survival or response to platinum-based chemotherapy is still unclear.

It's possible that additional determinants besides molecular and histological features are associated with cancer aggressiveness and resistance to chemotherapy agents, including the different compliance of cancer tissues with respect to healthy ones. To this respect, a physical technique, named the atomic force microscopy (AFM), is emerging as a new tool in pathology to study the mechanical properties of tumors and further define their heterogeneity.[13]

In the present study, we tested the diagnostic potential of AFM and its possible utility in ovarian cancer pathology by analyzing the biomechanical properties of certain HGSOCs growing patterns directly on standard H&E tissue sections.

Methods

Sample collection

Samples were collected at the National Cancer Institute of Aviano (C.R.O.). All patients gave informed consent before enrollment in the study and ethical approval for the study was obtained by the institutional review board (protocol number 1213, 24 January 2017). The criteria for patient's selection were: i) women who had stage IIIC or IV high grade serous ovarian cancer, ii) the availability of partial or complete follow-up information and iii) the availability of H&E slides and corresponding formalin-fixed and paraffin-embedded tissue blocks.

Histological and immunohistochemical revision

Histological revision and immunohistochemical staining were carried out to confirm HGSOC diagnosis and investigate tumor growth. In particular, IHC analysis was carried out using a panel of seven biomarkers modified by Kobel et al[5] which allows discriminating HGSOC from other types of epithelial ovarian cancer. The list of the biomarkers and their analytical details are reported in Table 1. After diagnostic confirmation, eighteen samples were chosen according to the HGSOC growing patterns described by Soslow et al.[14] All selected cases were HGSOC peritoneal implants derived from debulking procedures carried out between 2010 and 2016 for which complete or partial clinical information was available. Since different HGSOC architectural patterns often coexist in the same tumor specimen, only samples with pure morphological architecture or one evident predominant pattern were taken into consideration. The architectural patterns selected for AFM analysis included papillary, micropapillary, solid, transitional-like and endometrioid-like. As healthy controls stromal tissues derived from two peritoneal locations were chosen.

In addition to the pattern analysis, a histopathological characterization of the tissue slides by visual estimation was carried out as well, in order to relate tumor stiffness with histological parameters such as the degree of vascular invasion (0-3 score), necrosis (0-3 score), the number of mitoses (×10 HPF) and the number of lymphocytes (×1 HPF).

Table 1
Antibodies used for immunohistochemical analysis.

Antibody	Clone	Localization	Incubation
p53	DO-7 Ventana	Nuclear	16 min 37° C
p16	E6H4 Ventana	Nuclear/cytoplasm	16 min 36° C
WT1[a]	6F-H2 Ventana	Nuclear	40 min 37° C
Ki67	30-9 Ventana	Nuclear	16 min 37° C
PR[b]	1E2 Ventana	Nuclear	16 min 36° C
HNF1β[c]	HPA002083-Sigma	Nuclear	32 min RT
BRCA1	MS110 Abcam	Nuclear/cytoplasm	36 min RT

[a] WT1: Wilm's tumor protein 1.
[b] PR: progesterone receptor.
[c] HNF1β: hepatocyte nuclear factor 1-β.

TMA construction

In order to perform AFM analyses, tissue microarrays were constructed using FFPE tissue blocks of the selected peritoneal implants. For each block, one to three representative spots of the lesion were taken, using as reference the respective spots marked on H&E slides. Tissue cores of 1.2 mm diameter were drawn off from the selected spots of the donor paraffin blocks and punched into a recipient block using an Arraymold tissue Microarrayer (Riverton, Utah, USA). Once prepared, TMA was placed upside-down into a glass slide at 40 °C overnight to allow incorporation of tissue cores into the paraffin block. After cooling, 4 μm thick sections were cut and stained according to the Institute's standard processing protocol.

AFM measurements

The stiffness of tissues sections as small as 4 μm in thickness was studied by determining the Young's modulus of cells visualized inside the tissue. Measurements were made directly on TMA slides in a liquid environment, using a Smena AFM (NT-MDT Co., Moscow, Russia) mounted on an inverted microscope (Nikon Eclipse Ti-U). The slide was placed in a 60-ml petri dish above the AFM stage for positioning the indentation locations during the experiments. Optical images were acquired on the inverted microscope using the software NIS Elements. Subsequently, the slide was immobilized on a plate by applying a two components fast drying glue (Reprorubber® Thin Pour). Afterwards, the petri dish was placed on the microscope stage within the plate and filled with PBS solution at room temperature.

Mechanical characterization tests were performed via force spectroscopy method, using AFM cantilever (Etalon HA-NC) with nominal spring constant of 3.5 N/m and a spherical polystyrene bead of 20 μm diameter glued at its terminal end. In order to characterize the spring constant of the cantilever, the thermal noise method was used while the sensitivity was measured over the rigid surface of the glass slide at the end of each experiment. The force–displacement curves were recorded accordingly using NOVA-Px 3.4 control and the analysis software (NT- MDT Co., Moscow, Russia). In each sample's

spot, one to three regions of interest (ROI) were selected, and in each region, over 40 points in an area of 300 × 400 μm^2 were measured (see Supplementary Figure 1). Young's modulus values, in kPa, were determined by fitting the force-displacement curves with a Hertzian model, taking advantage of the software AtomicJ.[15] All steps of the experiment, from the preparation of the samples up to the measurement of the mechanical characteristics, were carried out within a few hours.

Force–displacement curves fitting

In order to evaluate the Young's modulus in each indented point, force–displacement curves were fitted to the Hertzian model, which is widely used for the determination of elastic properties of cells from AFM force–indentation curves.[13] Hertzian model assumes the sample to be isotropic and linear elastic half-space, while the indenter is not deformable and interacting with the sample only mechanically. With respect to other contact mechanics models, as Derjaguin–Müller–Toporov, Johnson–Kendall–Roberts or non-Hertzian models,[17] which include for instance sample adhesion, the Hertz approximation is well suitable for the limit of small indentation depths. In our case, given the sample thickness of 4 μm, we analyzed an indentation depth of 200 nm from the contact point. The relation between the acting force F_0 of the indenter the substrate's Young's modulus E and the indentation depth δ in the Hertz model is then:

$$F_0 = \frac{4}{3}\frac{ER^{1/2}A]^{3/2}}{1-\nu^2},$$

where ν is the Poisson's ratio and R the indenter's radius, with $\delta \ll R$.[16] We assume a Poisson's ratio of 0.5, as for soft materials where the bulk modulus is largely exceeding the shear modulus.

Common to all the contact mechanics models is that they neglect the effect of back-reflection of the stress transmitted from the probe to the stiff substrate on which cell/tissues are lying to the sample and then to the cantilever itself, introducing errors in the sample elastic modulus evaluation. We therefore decided to include a bottom effect correction term as suggested by Dimitriadis et al[18] resulting in the following expression for the indentation force:

$$F = F_0\left[\frac{1}{h^0} + \frac{1.133(\delta R)^{\frac{1}{2}}}{h} + \frac{1.497\delta R}{h^2} + \frac{1.469(\delta R)^{\frac{3}{2}}}{h^3} + \frac{0.755(\delta R)^2}{h^4}\right]$$

This modified Hertzian contact model, valid for spherical probes, allowed us to improve the quality of the fit, as controlled by maximizing the coefficient of determination R^2.[19]

Statistical tests

Mann–Whitney test was used to compare Young's modulus among HGSOC patterns and healthy tissue. The mean Young's modulus of each sample has also been calculated to correlate sample's stiffness with clinical and histological variables. The obtained values were dichotomized for subsequent analysis with respect to their median value. Values lower and equal or higher than the median value were classified as "low" or "high" status, respectively. The "low" and "high" groups were then compared with clinical and histological variables using contingency tables and Chi-square test while their prognostic significance was assessed using the log-rank test and plotted using the Kaplan–Meier curves.

Table 2
Clinicopathologic features of patients.

Variable	*n* (%), mean
Age at diagnosis	60
FIGO stagea	
IIIC	11 (65)
IV	6 (35)
NA[b]	1
Survival	
Dead	9 (50)
Alive	9 (50)
Surgical strategy	
PDS[c]	16 (89)
NACT[d]	2 (11)
Primary platinum response	
Never progressed	3 (20)
Sensitive	9 (60)
Resistant	3 (20)
NA	3
Residual tumor after surgery	
Yes	14 (82)
No	3 (18)
NA	1

[a] FIGO stage: International Federation of Gynecology and Obstetrics staging system.
[b] NA: data not available.
[c] PDS: primary debulking surgery.
[d] NACT: neo-adjuvant chemotherapy

Results

Clinicopathological features of the patients

A summary of the clinicopathological features of the eighteen patients selected is reported in Table 2.

Stiffness of HGSOC architectural patterns

Young's modulus of 20 tissues samples including 18 tumors and two healthy controls was measured by indentation in one to three different locations within each TMA's tissue spot. HGSOC tissue samples were chosen according to the architectural pattern; in detail, 3 endometrioid-like, 4 micropapillary-like, 4 papillary, 4 solid and 3 transitional-like high grade serous ovarian carcinomas were analyzed. A representative image of each morphological pattern and a healthy peritoneal tissue is depicted in Figure 1.

For each sample, a mean of 51 indentations over the selected locations was performed. Due to samples' heterogeneity a portion of the acquired curves was remeasured during the experiment and another portion was deemed unfit for the further analysis at the following steps.

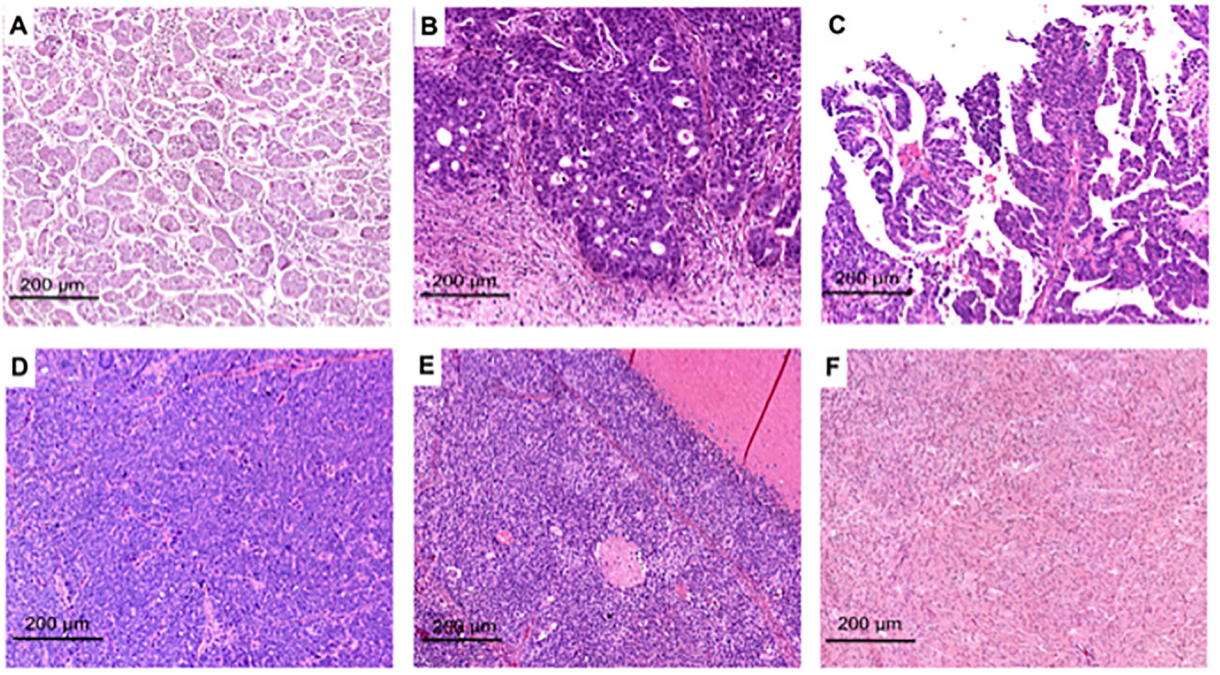

Figure 1. Representative optical microscope images of HGSOC patterns **(A-E)** and healthy peritoneal tissue **(F)**. HGSOC patterns: micropapillary-like **(A)**; endometrioid-like **(B)**; papillary **(C)**; solid **(D)**; transitional-like **(E)**; and healthy peritoneal fibrous tissue **(F)**.

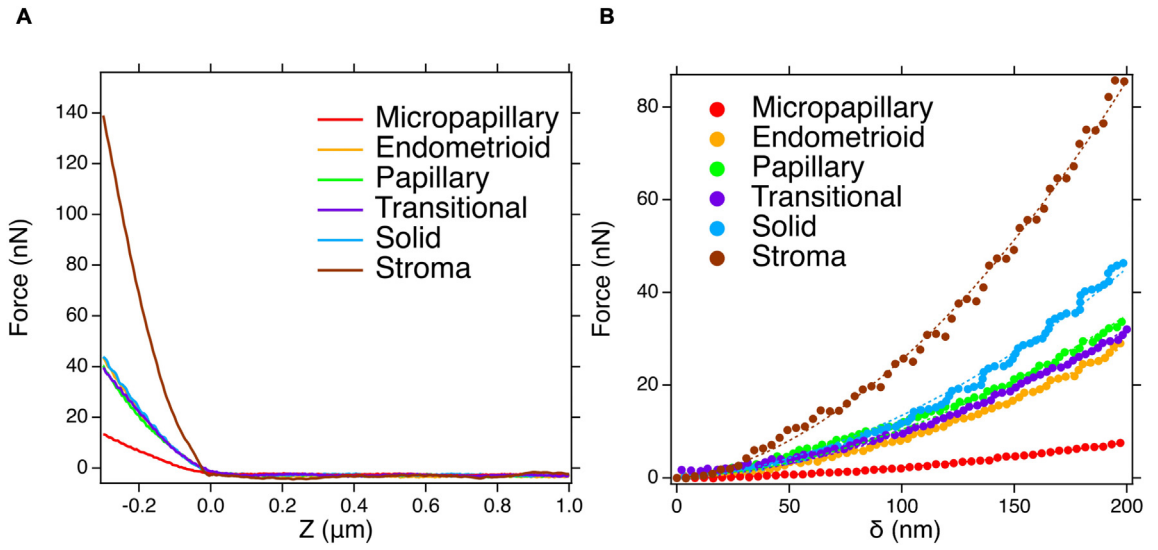

Figure 2. Representative curves of AFM force vs distance **(A)** and vs sample indentation **(B)** for the HSOGC patterns and healthy peritoneal tissue. In **B** dots show experimental force curves, and dashed lines are the curves fitted by the applied Hertz model.

Stiffness values derived from the two healthy controls and from tumors with the same architectural pattern were gathered and analyzed.

In Figure 2 we report the representative AFM force–distance and corresponding force–indentation curves with modified Hertz fit to extract the Young's modulus for the 5 different HGSOC architectural patterns and for the control (stroma).

Due to heterogeneity of tissue morphology, the outlier stiffness values were removed from each group using ROUT (Robust regression and outlier removal) method on Prism software and setting the maximum desired FDR (false discovery rate) to 10%. Cleaned data for each group were then analyzed for the distribution of elastic moduli and fit to the Gaussian model.

Among the five tumor patterns, solid and transitional-like ones showed a broad distribution of stiffness values compared to the other three patterns, ranging from 5 to 145 kPa for the solid pattern and from 5 to 105 kPa for transitional-like tumors. Multi-gaussian peak fit gave values centered at 23, 66 and 100 kPa for solid tumor (23 kPa the prevalent one) and 10, 42 and 98 kPa (98 the weakest peak) for the transitional pattern, respectively.

Papillary and endometrioid-like architectures had almost the same trend; in both groups the prevalent gaussian peaks were

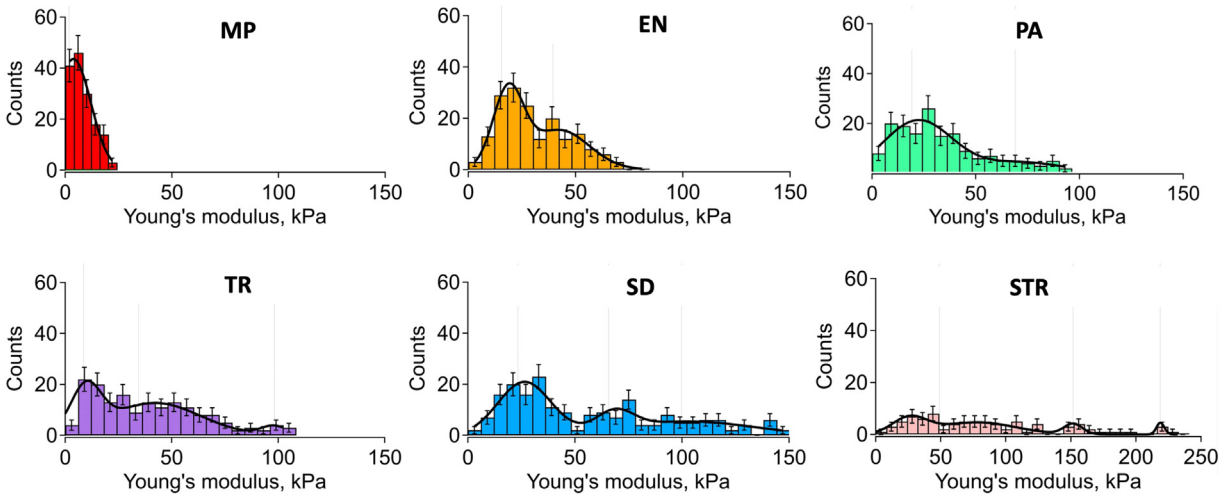

Figure 3. Frequency distribution with standard errors of Young's modulus in HGSOC patterns and stromal control. MP = micropapillary-like; EN = endometrioid like; PA = papillary; TR = transitional-like; SD = solid; STR = stroma.

Table 3
Fit results for the Young's modulus of the analyzed tumor patterns and the healthy controls.

	Peak position (kPa)	FWHM[a] (kPa)	Amplitude ± st.dev.
Tumor pattern			
Endometrioid-like	15.5	16.7	30 ± 5
	39.5	32.6	15 ± 2
Micropapillary	1.8	19.2	44 ± 3
Papillary	19.2	38.9	21 ± 3
	69.1	48.8	4 ± 2
Solid	23.3	29.0	20 ± 3
	65.7	20.5	7 ± 6
	99.8	71.5	5 ± 2
Transitional-like	9.73	16.7	17 ± 4
	42.1	50.1	13 ± 2
	98.1	14.0	4 ± 3
Healthy tissue			
Stroma	26.1	31.0	6 ± 2
	77.7	69.0	4.7 ± 0.7
	151.8	16.6	4 ± 1
	218.8	6.7	5 ± 4

[a] Full width at half maximum

centered around 17 kPa on average, but the range was slightly broader in the first one (5-90 kPa) when compared to the latter (0-70 kPa).

Micropapillary-like pattern instead, presented a very narrowed distribution of Young's moduli (range 0-20 kPa) with almost 40% of the occurrences detected at 5 kPa; moreover, its gaussian peak was centered at 2 kPa (single gaussian fit), rendering it by far the softest among the tumor architectures analyzed.

Lastly, the peritoneal fibrous tissues used as healthy controls were the hardest when compared to HGSOC specimens, displaying also a remarkable broader range of distribution. Stiffness values were comprised between 10 and 230 kPa while gaussian peaks were placed at 26, 78, 152 and 219 kPa (multi-gaussian fit). The quantitative analysis of the stiffness distribution for HGSOC patterns and healthy tissues is represented as histograms in Figure 3 and the exact fitting values are reported in Table 3.

AFM discriminates between HGSOC morphologies

In order to investigate on the ability of AFM to discriminate between each single HGSOC pattern, *t* test comparison was performed. The mean elastic modulus, expressed in kPa, was 8.1 (± 0.4) for micropapillary-like HGSOC, 30.3 (± 1.2) for endometrioid-like, 33.4 (± 1.7) for papillary, 39 (± 2) for transitional-like and 56.8 (± 2.7) for solid HGSOC. In healthy peritoneal stroma the mean value was 85.3 (± 6.2). Results of *t* test comparison between each group did not show differences in the mean elastic modulus between papillary and endometrioid tumors ($P = 0.4$) and between papillary and transitional-like tumors ($P = 0.1$). Nonetheless, a strong and significant difference was found between Young's moduli for all the other architectural patterns. Moreover, as expected, all tumor patterns were significantly softer compared to the stromal controls (Figure 4).

Stiffness is related to FIGO stage

Sample's stiffness was compared with histological and clinicopathological variables, using the mean Young's modulus of each sample. No significant associations were found between the stiffness and the response to chemotherapy, optimal cytoreduction or the histological parameters. Nevertheless, a trend toward worse outcome was seen in patients with softer tumors compared to those with harder ones ($P = 0.06$) (Figure 5, *D*).

Patients with FIGO stage IIIC had a different and broader distribution of Young's moduli when compared to those at stage IV. Multi-gaussian peak fit gave values centered at 15 and 47 kPa for the first group and 3 and 18 kPa for the second one (Figure 5, *A* and *B*). Moreover, *t* test comparison showed that patients with stage IV disease had significantly softer tumors compared to those at earlier stage ($P = 0.03$) (Figure 5, *C*).

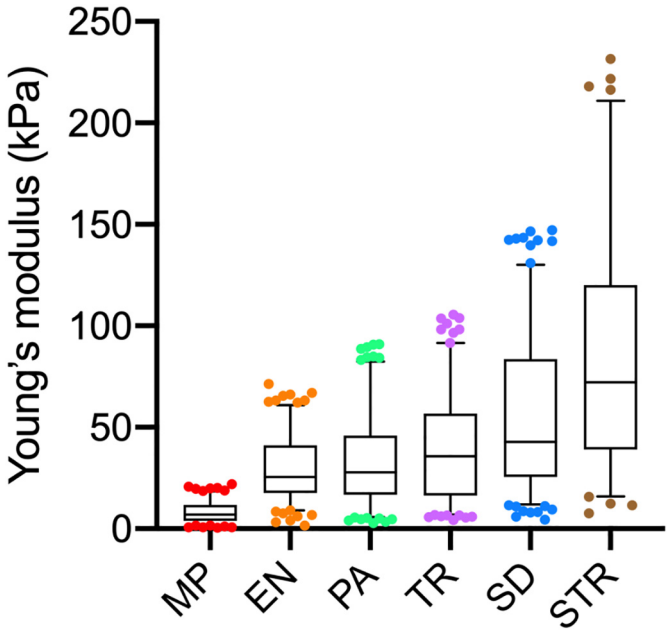

Figure 4. Boxplots of Young's moduli for each architectural pattern and stromal control. MP = micropapillary-like; EN = endometrioid like; PA = papillary; TR = transitional-like; SD = solid; STR = stroma.

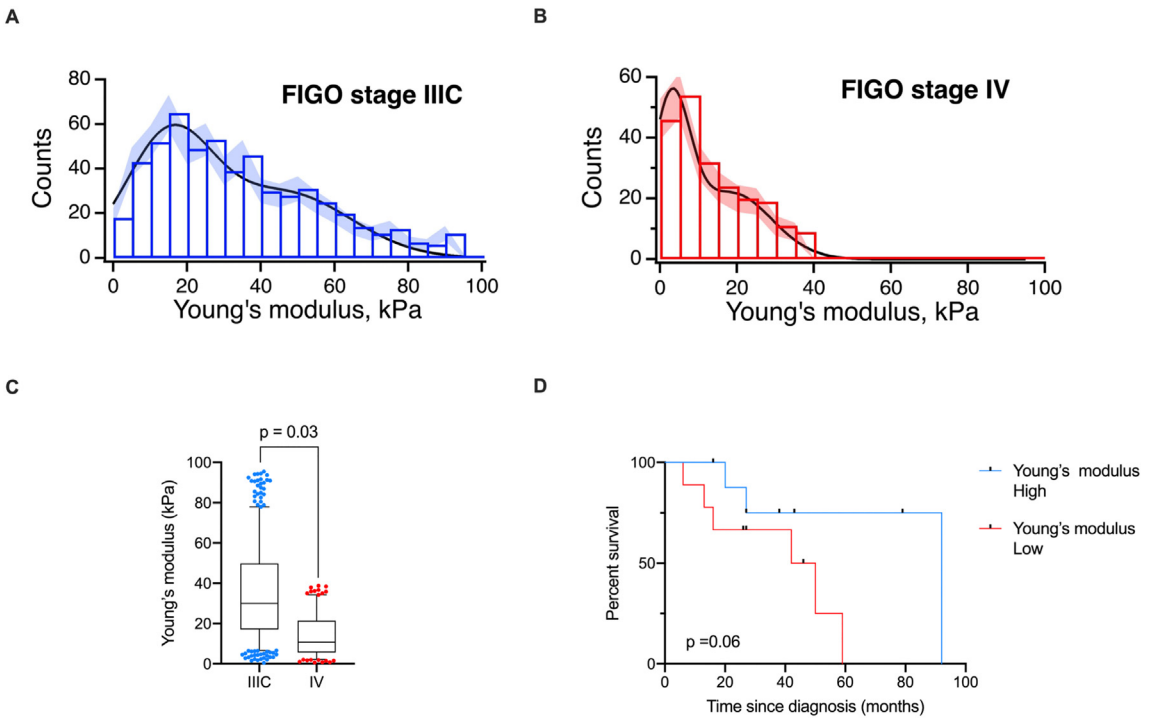

Figure 5. Frequency distribution of stiffness values in patients with FIGO stage IIIC **(A)** and IV **(B)**. Boxplots of Young's moduli in patients having HGSOC at different FIGO stage **(C)**. Stiffness-related overall survival (OS) represented as Kaplan–Meier curves (D).

Discussion

Pathologists are aware that high grade serous ovarian cancer presents a variety of growing patterns, often coexisting in the same tumor sample. However, so far none of these patterns has shown a particular histologic or molecular feature indicative of patients' prognosis.

In the last years, a growing number of studies have shown that cancer tissues can be characterized also by their mechanical proprieties using physical techniques such as the atomic force

microscopy (AFM).[13] The use of AFM for characterizing tissue stiffness in clinical samples has successfully led to identification of nanomechanical signatures associated with healthy, pre-cancerous and cancerous conditions in different tissues,[20,21] including ovaries.[22]

In our study, we have characterized nanomechanically five different HGSOC morphological patterns and detected an association between tumor stiffness and morphology. In particular, HGSOCs presenting micropapillary-like morphology were those with the lowest mean level of stiffness while those with solid features had the highest stiffness values, closer to that of healthy tissues.

The stiffness of living cancerous cells has been already linked to their metastatic potential in different type of tumors[23–25] including ovarian ones.[26] In the scientific community there's a general agreement in describing among cancer cells those with lower stiffness having higher invasive potential when compared to the stiffer ones. Accordingly, our results, obtained in a clinical tissue context, pointed out that the micropapillary-like morphology, could represent a particular aggressive entity in the spectrum of HGSOCs since it has by far the lowest Young's modulus compared to all other architectures. Micropapillary infiltrative pattern in peritoneal metastases has already been associated with poor outcome in agreement with our findings.[27]

Nonetheless, different or even opposite results have been reported in literature about the relationship between tumor stiffness and metastatic potential at the tissue level or at the single cell level. Several authors have addressed that elasticity measurements on tissue sections can rather be the results of both cancer and stromal component contributions. In particular, the extracellular matrix could be characterized by a broader distribution of stiffness values compared to tumor epithelium.[28–30] In agreement to these results, the distribution of Young's moduli in our healthy peritoneal controls, composed primarily of matrix fibers, was notably broader than HGSOC specimens. To this regard, to minimize the effect of the stromal component in cancer samples assessment, we used tissue microarrays of pre-selected tumor-enriched regions; moreover, indentation measurements were performed only on tumor epithelial components avoiding further potential confounding factors such as the necrotic areas.[31]

In agreement with Plodinec et al on breast cancer models,[30] our results also highlighted that patients with stage III disease had significantly stiffer tumors in comparison to those at stage IV, suggesting a general tendency of all HGSOCs patterns to decrease their stiffness during disease progression and increase their invasive capacity. In addition, although we couldn't perform a log rank test analysis stratified by HGSOC patterns due to limited number of samples, we found a borderline association between the mean levels of stiffness and patients' overall survival ($P = 0.06$).

In our study, the biomechanical proprieties of HGSOC architectural patterns have been assessed in FFPE debulking material as normally processed in the surgical pathology unit. Limited data are reported in literature on the effect of fixatives, and in particular formalin, on AFM indentation measurements. However, most studies reporting experimental data on aldehyde-based fixatives, usually paraformaldehyde and glutaraldehyde, have shown an evident increase in stiffness in fixed tissues compared to fresh or frozen ones.[32,33] This is an expected result, given the crosslinking effect of aldehyde-based fixation. In particular, Nurgazizov and colleagues, comparing the effect of both formalin and glutaraldehyde on the stiffness of rat erythrocytes, have shown that the increase in Young's modulus was lower in formalin than in glutaraldehyde fixation with respect to the fresh cell control.[34] In addition, Codan et al showed that stiffness ratios between healthy and cancer cells were maintained also after fixation and that the relation can be described by means of a coefficient.[35] Our study is monocentric; therefore, all the specimens were collected in the same cancer Institute and were all fixed in formalin according to the hospital standardized procedures. Consequently, we are confident in hypothesizing that the intra-samples stiffness relationship was maintained after the fixation procedure.

We acknowledge as a limitation of our study the small sample size and the lack of fresh or frozen tissues for matched samples comparison. Furthermore, we assessed tissues stiffness in samples with pure morphological patterns, but different HGSOC patterns often coexist in the same specimen. Therefore, in samples having multiple architectures further analyses are needed in order to verify if different biomechanical profiles can be discriminated and can help in the diagnostic process.

In conclusion, our study has shown that the use of AFM analysis can be an additional tool in HGSOC diagnosis since the biomechanical proprieties of these type of tumors and consequently their metastatic potential can be strictly related to their architectural patterns and tumor staging. Furthermore, our results have shown that the possible acquisition of tumor stiffness in clinical cancer samples could be an additional variable to help patients' prognostication.

Author contributions

Study conception and design: E. Azzalini, S. Bonin., L. Casalis, P. Parisse.

Acquisition of data: N. Abdurakhmanova, E. Azzalini, M. Bartoletti, V. Canzonieri, G. Stanta.

Analysis and data interpretation: E. Azzalini, N. Abdurakhmanova, S. Bonin, L. Casalis, P. Parisse.

Drafting of manuscript: E. Azzalini, N. Abdurakhmanova, S. Bonin

Critical revision: M. Bartoletti, V. Canzonieri, L. Casalis, G. Stanta, P. Parisse.

Appendix A. Supplementary data

Supplementary data to this article can be found online at https://doi.org/10.1016/j.nano.2021.102452.

References

1. Prat J. Ovarian carcinomas: five distinct diseases with different origins, genetic alterations, and clinicopathological features. *Virchows Arch* 2012; 460: 237-249. 2012/02/11. DOI: 10.1007/s00428-012-1203-5.
2. Vaughan S, Coward JI, Bast RC, Jr., et al. Rethinking ovarian cancer: recommendations for improving outcomes. *Nat Rev Cancer* 2011; 11: 719-725. 2011/09/24. DOI: 10.1038/nrc3144.

3. Macintyre G, Goranova TE, Silva DD, et al. Copy-number signatures and mutational processes in ovarian carcinoma. *bioRxiv* 2017174201, https://doi.org/10.1101/174201.
4. Tothill RW, Tinker AV, George J, et al. Novel molecular subtypes of serous and endometrioid ovarian cancer linked to clinical outcome. *Clinical Cancer Research* 2008;**14**:5198-208, https://doi.org/10.1158/1078-0432.Ccr-08-0196.
5. Kobel M, Bak J, Bertelsen BI, et al. Ovarian carcinoma histotype determination is highly reproducible, and is improved through the use of immunohistochemistry. *Histopathology* 2014; 64: 1004-1013. 2013/12/18. DOI: 10.1111/his.12349.
6. Kobel M, Rahimi K, Rambau PF, et al. An immunohistochemical algorithm for ovarian carcinoma typing. *Int J Gynecol Pathol* 2016; 35: 430-441. 2016/03/15. DOI: 10.1097/PGP.0000000000000274.
7. Coleman RL, Oza AM, Lorusso D, et al. Rucaparib maintenance treatment for recurrent ovarian carcinoma after response to platinum therapy (ARIEL3): a randomised, double-blind, placebo-controlled, phase 3 trial. *Lancet* 2017; 390: 1949-1961. 2017/09/17. DOI: https://doi.org/10.1016/S0140-6736(17)32440-6.
8. Murakami R, Matsumura N, Mandai M, et al. Establishment of a novel histopathological classification of high-grade serous ovarian carcinoma correlated with prognostically distinct gene expression subtypes. *Am J Pathol* 2016; 186: 1103-1113. 2016/03/20. DOI: 10.1016/j.ajpath.2015.12.029.
9. Kalimuthu NS, Wilson GW, Grant RC, et al. Morphological classification of pancreatic ductal adenocarcinoma that predicts molecular subtypes and correlates with clinical outcome. *Gut* 2020; 69: 317-328. 2019/06/16. DOI: 10.1136/gutjnl-2019-318217.
10. Shia J, Schultz N, Kuk D, et al. Morphological characterization of colorectal cancers in The Cancer Genome Atlas reveals distinct morphology-molecular associations: clinical and biological implications. *Mod Pathol* 2017; 30: 599-609. 2016/12/17. DOI: 10.1038/modpathol.2016.198.
11. Howitt BE, Hanamornroongruang S, Lin DI, et al. Evidence for a dualistic model of high-grade serous carcinoma: BRCA mutation status, histology, and tubal intraepithelial carcinoma. *Am J Surg Pathol* 2015; 39: 287-293. 2015/01/13. DOI: 10.1097/PAS.0000000000000369.
12. Ritterhouse LL, Nowak JA, Strickland KC, et al. Morphologic correlates of molecular alterations in extrauterine Mullerian carcinomas. *Mod Pathol* 2016; 29: 893-903. 2016/05/07. DOI: 10.1038/modpathol.2016.82.
13. Stylianou A, Lekka M, Stylianopoulos T. AFM assessing of nanomechanical fingerprints for cancer early diagnosis and classification: from single cell to tissue level. *Nanoscale* 2018;**10**:20930-45, https://doi.org/10.1039/c8nr06146g.
14. Soslow RA, Han G, Park KJ, et al. Morphologic patterns associated with BRCA1 and BRCA2 genotype in ovarian carcinoma. *Mod Pathol* 2012; 25: 625-636. 2011/12/24. DOI: 10.1038/modpathol.2011.183.
15. Hermanowicz P, Sarna M, Burda K, et al. AtomicJ: an open source software for analysis of force curves. *Rev Sci Instrum* 2014; 85: 063703. 2014/07/06. DOI: 10.1063/1.4881683.
16. Hertz H. Ueber die Berührung fester elastischer Körper. *Journal für die reine und angewandte Mathematik* 1882;**1881**:156-71, https://doi.org/10.1515/crll.1882.92.156.
17. Krieg M, Fläschner G, Alsteens D, et al. Atomic force microscopy-based mechanobiology. *Nat Rev Phyc* 2019;**1**:41-57 Reviewhttps://doi.org/10.1038/s42254-018-0001-7.
18. Dimitriadis EK, Horkay F, Maresca J, et al. Determination of elastic moduli of thin layers of soft material using the atomic force microscope. *Biophys J* 2002;**82**:2798-810, https://doi.org/10.1016/S0006-3495(02)75620-8.
19. Gavara N. Combined strategies for optimal detection of the contact point in AFM force-indentation curves obtained on thin samples and adherent cells. *Sci Rep* 2016; 6: 21267. 2016/02/20. DOI: 10.1038/srep21267.
20. Lopez JI, Kang I, You WK, et al. In situ force mapping of mammary gland transformation. *Integr Biol-Uk* 2011;**3**:910-21, https://doi.org/10.1039/c1ib00043h.
21. Tian MX, Li YR, Liu WR, et al. The nanomechanical signature of liver cancer tissues and its molecular origin. *Nanoscale* 2015;**7**:12998-3010, https://doi.org/10.1039/c5nr02192h.
22. Ansardamavandi A, Tafazzoli-Shadpour M, Omidvar R, et al. An AFM-based nanomechanical study of ovarian tissues with pathological conditions. *Int J Nanomedicine* 2020; 15: 4333-4350. 2020/07/02. DOI: 10.2147/IJN.S254342.
23. Cross SE, Jin YS, Rao J, et al. Nanomechanical analysis of cells from cancer patients. *Nat Nanotechnol* 2007; 2: 780-783. 2008/07/26. DOI: 10.1038/nnano.2007.388.
24. Lekka M, Laidler P, Gil D, et al. Elasticity of normal and cancerous human bladder cells studied by scanning force microscopy. *Eur Biophys J* 1999; 28: 312-316. 1999/07/08. DOI: 10.1007/s002490050213.
25. Lekka M, Pogoda K, Gostek J, et al. Cancer cell recognition—mechanical phenotype. *Micron* 2012; 43: 1259-1266. 2012/03/23. DOI: 10.1016/j.micron.2012.01.019.
26. Xu W, Mezencev R, Kim B, et al. Cell stiffness is a biomarker of the metastatic potential of ovarian cancer cells. *PLoS One* 2012; 7: e46609. 2012/10/12. DOI: 10.1371/journal.pone.0046609.
27. Hussein YR, Ducie JA, Arnold AG, et al. Invasion patterns of metastatic extrauterine high-grade serous carcinoma with BRCA germline mutation and correlation with clinical outcomes. *Am J Surg Pathol* 2016; 40: 404-409. 2015/11/18. DOI: 10.1097/PAS.0000000000000556.
28. Ansardamavandi A, Tafazzoli-Shadpour M, Omidvar R, et al. Quantification of effects of cancer on elastic properties of breast tissue by atomic force microscopy. *J Mech Behav Biomed Mater* 2016; 60: 234-242. 2016/02/16. DOI: 10.1016/j.jmbbm.2015.12.028.
29. Lekka M, Gil D, Pogoda K, et al. Cancer cell detection in tissue sections using AFM. *Arch Biochem Biophys* 2012; 518: 151-156. 2012/01/03. DOI: 10.1016/j.abb.2011.12.013.
30. Plodinec M, Loparic M, Monnier CA, et al. The nanomechanical signature of breast cancer. *Nat Nanotechnol* 2012; 7: 757-765. 2012/10/23. DOI: 10.1038/nnano.2012.167.
31. Ciasca G, Sassun TE, Minelli E, et al. Nano-mechanical signature of brain tumours. *Nanoscale* 2016; 8: 19629-19643. 2016/11/18. DOI: 10.1039/c6nr06840e.
32. Hutter JL, Chen J, Wan WK, et al. Atomic force microscopy investigation of the dependence of cellular elastic moduli on glutaraldehyde fixation. *J Microsc* 2005; 219: 61-68. 2005/09/15. DOI: 10.1111/j.1365-2818.2005.01497.x.
33. Zemla J, Stachura T, Gross-Sondej I, et al. AFM-based nanomechanical characterization of bronchoscopic samples in asthma patients. *J Mol Recognit* 2018; 31: e2752. 2018/07/19. DOI: https://doi.org/10.1002/jmr.2752.
34. Bukharaev AA, Mozhanova AA, Nurgazizov NI, et al. Measuring local elastic properties of cell surfaces and soft materials in liquid by atomic force microscopy. *Phys Low-Dimens Str* 2003;**3-4**:31-7.
35. Codan B, Martinelli V, Mestroni L, et al. Atomic force microscopy of 3T3 and SW-13 cell lines: an investigation of cell elasticity changes due to fixation. *Mater Sci Eng C Mater Biol Appl* 2013; 33: 3303-3308. 2013/05/28. DOI: https://doi.org/10.1016/j.msec.2013.04.009.